Available online at www.sciencedirect.com
SCIENCE DIRECT®
Physics and Chemistry of the Earth 28 (2003) 1229–1239
PHYSICS and CHEMISTRY of the EARTH
www.elsevier.com/locate/pce

Detection of spatial, temporal, and spectral surface changes in the Ny-Ålesund area 79° N, Svalbard, using a low cost multispectral camera in combination with spectroradiometer measurements

Jørgen Hinkler [a,*], Jon Børre Ørbæk [b,1], Birger Ulf Hansen [a,2]

[a] *Institute of Geography, University of Copenhagen, Øster Voldgade 10, 1350 Copenhagen K, Denmark*
[b] *Norwegian Polar Institute, P.O. Box 505, N-9171 Longyearbyen, Svalbard, Norway*

Received 30 January 2003; received in revised form 27 June 2003; accepted 5 August 2003

Abstract

Changes in surface reflection at the arctic tundra at Ny-Ålesund, Svalbard (79° N) were monitored during the melting season 2002 using a low cost multispectral digital camera with spectral channels similar to channels 2, 3, and 4 of the Landsat Thematic Mapper satellite sensor. The camera was placed 474 m above sea level at the Zeppelin Mountain Research Station and was programmed to take an image automatically every day at solar noon. To achieve areal consistency in the images (which is necessary for mapping purposes) the images were geometrically rectified into multispectral digital orthophotos. In contrast to satellite images with high spatial resolution the orthophotos provide data with high spatial *and* high temporal resolution at low cost. The study area covers approximately 2 km^2 and when free of snow, it mainly consists of typical high arctic tundra with patchy vegetation and bare-soil in between. The spectral information in the images was used to divide the rectified images into maps representing different surface classes (including three subclasses of snow). By combining classified image data and ground measurements of spectral surface reflectance, a methodology to produce daily maps of surface albedo was developed. The method takes into account the effect of decreasing snow-albedo with ageing snow pack, and the very rapid decrease of albedo when the snow pack is shallow (<10 cm) which is due to influence from the underlying ground. The time series of modelled albedo-maps shows that the snow melt period (when the albedo decreases from 80% to 20%) varies from less than 10 days in areas near the coast or in the Ny-Ålesund settlement till more than 70 days in areas with large snow or ice accumulations. For the entire study area the mean length of the 2002 melting period was 28.3 days with a standard deviation of 15.1 days. Finally, the duration of the snowmelt season at a location where it has been measured routinely since 1980, was calculated to 23 days, which is very close to what is the average for the last two decades.

Keywords: Remote sensing; Orthophoto; Multispectral; Snow; Albedo; Reflectance; Arctic; Svalbard; Ny-Ålesund; Digital; Camera

1. Introduction

Surface albedo is one of the most critical variables affecting the Earth's climate. Due to an extensive snow cover, surface albedo is normally high in arctic regions. However, in the short melting season, surfaces in these regions show a significant natural variability in reflectance, both with respect to its spectral variation, and in time and space. It is important to monitor and understand this natural variability, before using surface albedo for energy- and water balance modelling, ecological modelling of biophysical parameters and climate change research. In arctic areas the surface albedo drops from around 80% under fully snow covered conditions to bare ground levels (10–20%) within two to four weeks, and the date when the tundra becomes snow-free varies from early June till mid July (e.g. Hinkler et al., 2002; Winther et al., 1999). Thus, the changing spectral characteristics of the surface during melt-off combined with the rapid decrease in albedo call for cautious use of remote sensing-derived albedo, and a need for data recorded at frequent time intervals. Satellite remote-sensed data

* Corresponding author. Tel.: +45-35-32-41-68.
E-mail addresses: jh@geogr.ku.dk (J. Hinkler), orbak@npolar.no (J.B. Ørbæk), buh@geogr.ku.dk (B.U. Hansen).
[1] Tel.: +47-79-02-26-00/26-21.
[2] Tel.: +45-35-32-25-19.

1474-7065/$ - see front matter © 2003 Elsevier Ltd. All rights reserved.
doi:10.1016/j.pce.2003.08.059

have been used in a wide variety of arctic studies for almost three decades. For example, they have been used in snow and glacier studies by Jacobsen et al. (1993), and surface energy- and water balance by Soegaard et al. (2001). Multispectral satellite data from arctic areas have also been used to monitor and model the spatio-temporal variation of biophysical parameters such as length of growing season (e.g. Tamstorf, 2000), vegetation cover fraction (e.g. Jacobsen and Hansen, 1996), leaf area index and biomass production (e.g. Hansen, 1991). However, at smaller scales image data with high spatial resolution are required to produce a detailed picture of the spatial variation of surface reflection within a given area. This need cannot be fulfilled by using high resolution satellite data like Landsat Thematic Mapper (TM) or Système Probatoire pour l'Observation de la Terre (SPOT). This is due to the fact that the temporal resolution of these satellite systems is too poor to acquire images of the same area frequently. Furthermore, satellite images are sensitive to cloud cover and data with high spatial resolution are often costly.

This study was carried out in the area around Ny-Ålesund 79° N, Svalbard and had two main purposes. The first purpose was to develop and set up a low cost system to produce a time series of orthographically rectified multispectral images of the study area (Figs. 1 and 4) offering both high spatial and temporal resolution. The second purpose was to combine these images with field measurements of surface reflectance in order to compute a time series of daily albedo-maps and then use these for calculation and description of the spatial variability of snowmelt-duration within the study area. Furthermore it was an aim to reveal peculiar albedo features that are connected to different regimes of snow melt and different surface types.

The system producing the multispectral digital orthophotos (MDOs) consists of a Tetracam multispectral three channelled (green (G), red (R), near infrared (NIR)) digital camera (MDC), and a specially developed software package—Ortho (Have, 1999). The camera was placed at the Zeppelin Mountain Station at 474 m above sea level facing Ny-Ålesund/Kongsfjorden taking daily oblique images of the Ny-Ålesund area (Fig. 4). Every image recorded under fair weather conditions from this time series were orthographically rectified. Ground truth measurements for calibration and verification of surface reflectance were performed with a Fieldspec FR spectroradiometer.

The study area (which includes the Ny-Ålesund settlement) is limited by the field of view of the camera and the coastline along Kongsfjorden (Fig. 1), and it covers approximately 2 km^2. When free of snow, the surface in the area roughly consists of typical high arctic tundra with patchy vegetation and bare-soil/gravel in between. In a few spots some particularly dark surfaces, that

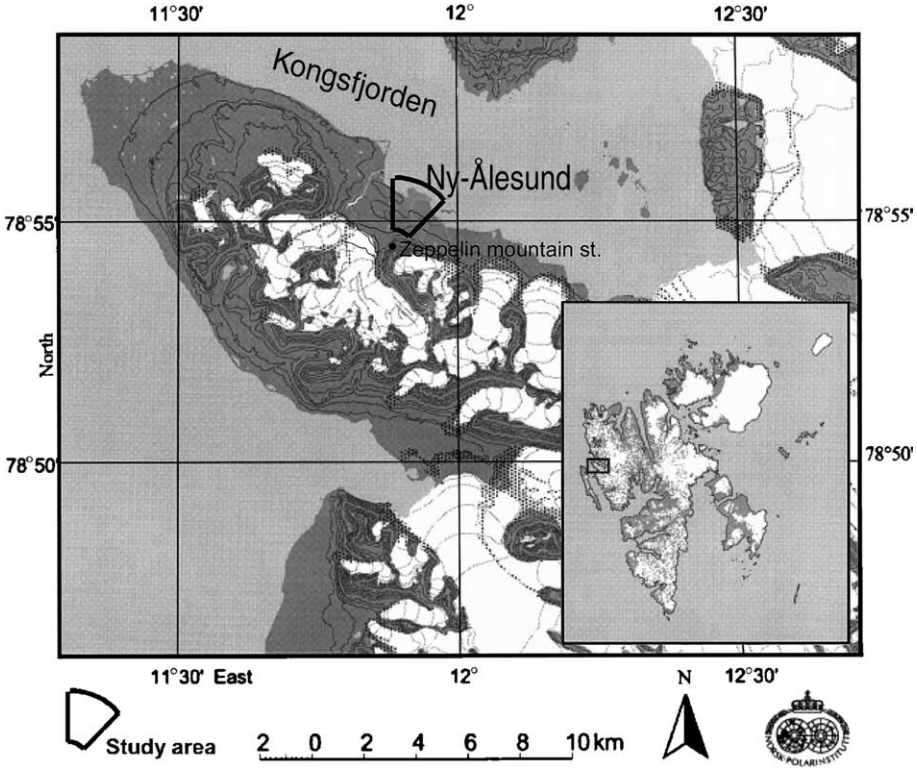

Fig. 1. Map of Kongsfjorden area, Svalbard. The study area (the area covered by the multispectral digital camera) is indicated by the black polygon.

are remnants from a former coal mining activity, are present.

2. Spectral properties of different surface types

In relation to remote sensing, natural surfaces can roughly be divided into four major different categories—bare-soil, vegetation, water and snow/ice. The spectral reflectance of bare-soil increases generally with wavelength, and is affected by the soil texture, moisture, and presence of organic matter. A coarse, wet and organic soil has a lower reflectance than a dry clay soil.

Vegetated surfaces have three distinct wavelength determined segments of reflectance. These can be characterized as low reflectance in the visible (400–700 nm) (VIS) part of the spectrum due to chlorophyll absorption, high reflectance in the near infrared (700–1200 nm) (NIR) part of the spectrum caused by cell structure and leaf area. In mid infrared (1200–2500 nm) vegetation has medium reflectance due to water absorption. The spectral reflectance of vegetation has a strong dependence of season as well as age and vegetation-type. The reflectance of water in VIS is a little higher than for vegetation and due to very high absorption, it declines to almost zero at higher wavelengths. The level of reflectance depends of depth and load of suspended material. Shallow water with suspended material has a high reflectance, while deep clear water has a very low reflectance.

The surface types of major interest in connection with this study are the snow covered surfaces. Snow is a matrix of ice grains, air, and water and often contains impurities like dust and plant materials. The optical properties of the snow pack in VIS and NIR depend on grain size distribution, thickness of the snow pack, occurrence of impurities and liquid water content (Warren, 1982). The reflectance from a fresh snow pack remains high in VIS, while a distinct drop occurs in NIR (Fig. 2) and finally it drops to below 10% in the mid-infrared region. The change from fresh to metamorphosed clean snow (which is due to crystal growth and increase of liquid water content) causes a reflectance decrease, especially at longer wavelengths. A further decrease in reflectance at wavelengths from 600–700 nm indicates that microscopic dust and other small particles may cover the snow surface, while macroscopic and visible dirt on the snow give a further decrease, mostly in the visible range (400–700 nm). Thinning of the snow causes a significant decrease in reflectance, as the underlying ground seems to become visible at a snow thickness of approximately 10 cm and less (Wiscombe and Warren, 1980).

Clouds highly increase the amount of diffuse radiation relative to the amount of direct radiation incident on a surface, and they also alter the spectral distribution

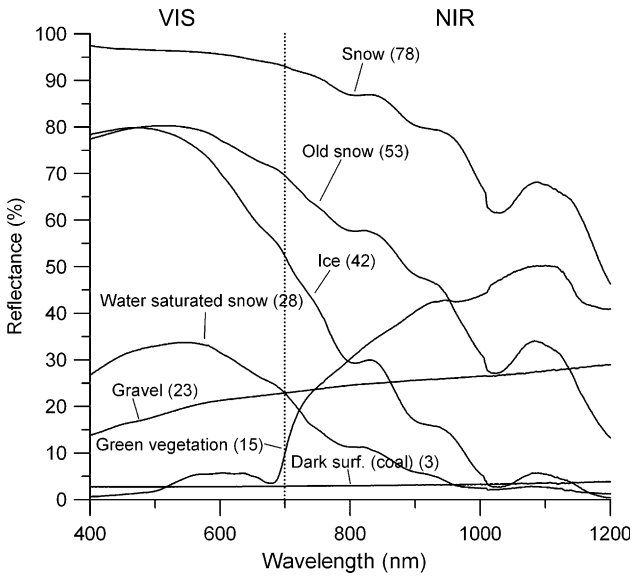

Fig. 2. Reflectance curves for seven different surface types (snow, old snow, ice, water, gravel, green vegetation, and dark surfaces—remnant from former coal deposits). All of the measurements were performed using a Fieldspec FR spectroradiometer. The numbers given in parenthesises are values of numerically integrated broad band albedo.

of the radiation reaching the surface, since they absorb a higher portion of infrared than visible radiation. Thus, a relatively high portion of visible radiation reaches the surface under cloudy conditions. Work by Winther et al. (1999) has shown that the combined effect of these factors can make the integrated broad band albedo increase with up to 7% in the case of a change from clear sky to 100% overcast conditions.

As metamorphosed snow reflects radiation anisotropically (Iqbal, 1983), the sensor derived albedo strongly depends on the geometry between the sun, the sensor and the surface segment (pixel). The reflectance of snow increases with illumination angle, especially for larger grains, because snow has a tendency to be strongly forward-scattering in NIR (Dozier, 1989). The increase in albedo can be as high as 25% and the largest anisotropy is seen for metamorphosed snow in measurements facing the sun.

As mentioned, reflectance of snow decreases in the NIR part of the spectrum. When attempting to divide snow into subclasses this decrease becomes of significant importance. As snow ages or melts, the grain size increases, and especially in NIR snow reflectance is sensitive to grain size. This means that the relative proportion between VIS and NIR is larger for old snow than for fresh snow, making it possible to separate fresh and metamorphosed snow. The normalized difference snow/ice index (NDSII) (De Abreau and LeDrew, 1997) is given by

$$\mathrm{NDSII} = \frac{\mathrm{VIS} - \mathrm{NIR}}{\mathrm{VIS} + \mathrm{NIR}}, \tag{1}$$

where VIS (580–680 nm) and NIR (725–1100 nm) are integrated reflectance values. The index ranges from −1 to 1, with snow and ice values expected between 0 and 1. The larger the index, the more metamorphosed the snow contained in the pixel in question. In this study the NDSII is used to distinguish between fresh and water saturated snow, and it was calculated using raw R and NIR pixel values.

3. Image data and field measurements

3.1. Multispectral digital camera images

The MDC is a Tetracam inc. single-CCD camera with a resolution of 1200×1024 pixels and a colour filter array applied to it. Thus each pixel on the CCD is sensitive to only one colour. After colour reconstruction (demosaicing processing using raw pixel data), the green, red, and near infrared (G, R, NIR) spectral bands approximately cover the following wavelength intervals: 520–570 nm (G), 600–690 nm (R), and 750–850 nm (NIR) (see Table 1).

The camera was set up inside the Zeppelin Mountain Research Station at 474 m above sea level facing a north to north-easterly direction towards the Ny-Ålesund settlement and Kongsfjorden (Fig. 4). The cameras internal alarm clock was programmed to trigger the camera and take a picture out through the window once a day during the period May 22–August 14. In order to obtain optimum light-conditions during image-exposure, the time of capture was set to be at solar noon. At that time of day the intensity of solar irradiation is at its maximum, and further, as the camera is pointed almost directly to the North (the same direction as the propagation of solar rays at noon) problems due to backlight and saturation can be avoided more easily. In addition to the daily images a diurnal time series was recorded at 10 min intervals at June 28–29.

This was done to investigate the cameras sensitivity to the solar azimuth angle. During the entire recording period, the local weather has varied with periods of fair weather conditions, periods with both high and low cloud cover, and periods with foggy conditions. Data were therefore recorded under a large number of different solar illuminations. Fig. 3(A)–(D) illustrate the MDCs response and dynamic range (in R and NIR) at different levels of solar illumination and at different azimuth angles. Fig. 3(A) and (B) reveal that image brightness is correlated to the global radiation and that the correlation is most significant at visible wavelengths. Note, around midnight the Sun's position is to the north, meaning that the solar rays propagate almost directly toward the camera lens. This explains the abrupt increase in pixel values at that time of day. The MDCs response is very sensitive to the adjustment of its diaphragm. During this study it has been attempted to adjust the diaphragm to cover light conditions varying from bright clear skies to overcast conditions. To avoid saturation on clear days, the diaphragm was set at a relatively high level. Thus, under overcast conditions, images were relatively dark, reducing the dynamic range of a given image significantly. In Fig. 3(C) and (D) the relation between global solar radiation, and the R, and NIR pixel values is shown (due to azimuth problems, data recorded during the time around midnight were excluded). From the figures, it can be observed that at the current diaphragm-settings a minimum of 250 and 400 $W m^{-2}$ (for R and NIR, respectively) is required to be able to discriminate two spectrally very different surface types without ambiguity (snow and vegetation) on the basis of a single spectral channel. Therefore (see Section 4.2), surface classification was based partly on relative proportions between spectral bands. The changing weather conditions combined with the MDCs high sensitivity to different illuminations has limited the number of images from the daily time series usable for surface classification to 19 out of a total of 85.

3.2. Field measurements

Spectral field data were collected during two field campaigns—the first one took place in mid May before extensive snowmelt began, and the second one at the end of June/beginning of July, where large vegetated areas and bare-soil areas were free of snow. Measurements were performed using a Fieldspec FR spectroradiometer (analytical spectral devices) measuring from 350 to 2500 nm. It consists of three built-in separate spectrometers. The first one measures from 350 to 1000 nm using a 512 element photodiode array, and has a spectral resolution of about 3 nm. The second and third ones are of scanning types and measure from 900 to 1850 nm and 1700 to 2500 nm, respectively sampling every 2 nm, with a spectral resolution of about 10 ± 11 nm. Results presented here primarily use data from the first spectro-

Table 1
The spectral channels of the Tetracam multispectral camera, the SPOT high resolution visible (HRV), and the Landsat TM satellite sensors

	MDC (nm)	SPOT (HRV) (nm)	Landsat TM (nm)
Green	520–570	Channel 1: 500–590	Channel 2: 520–600
Red	600–690	Channel 2: 610–680	Channel 3: 630–690
Near infrared	750–850	Channel 3: 790–890	Channel 4: 760–900

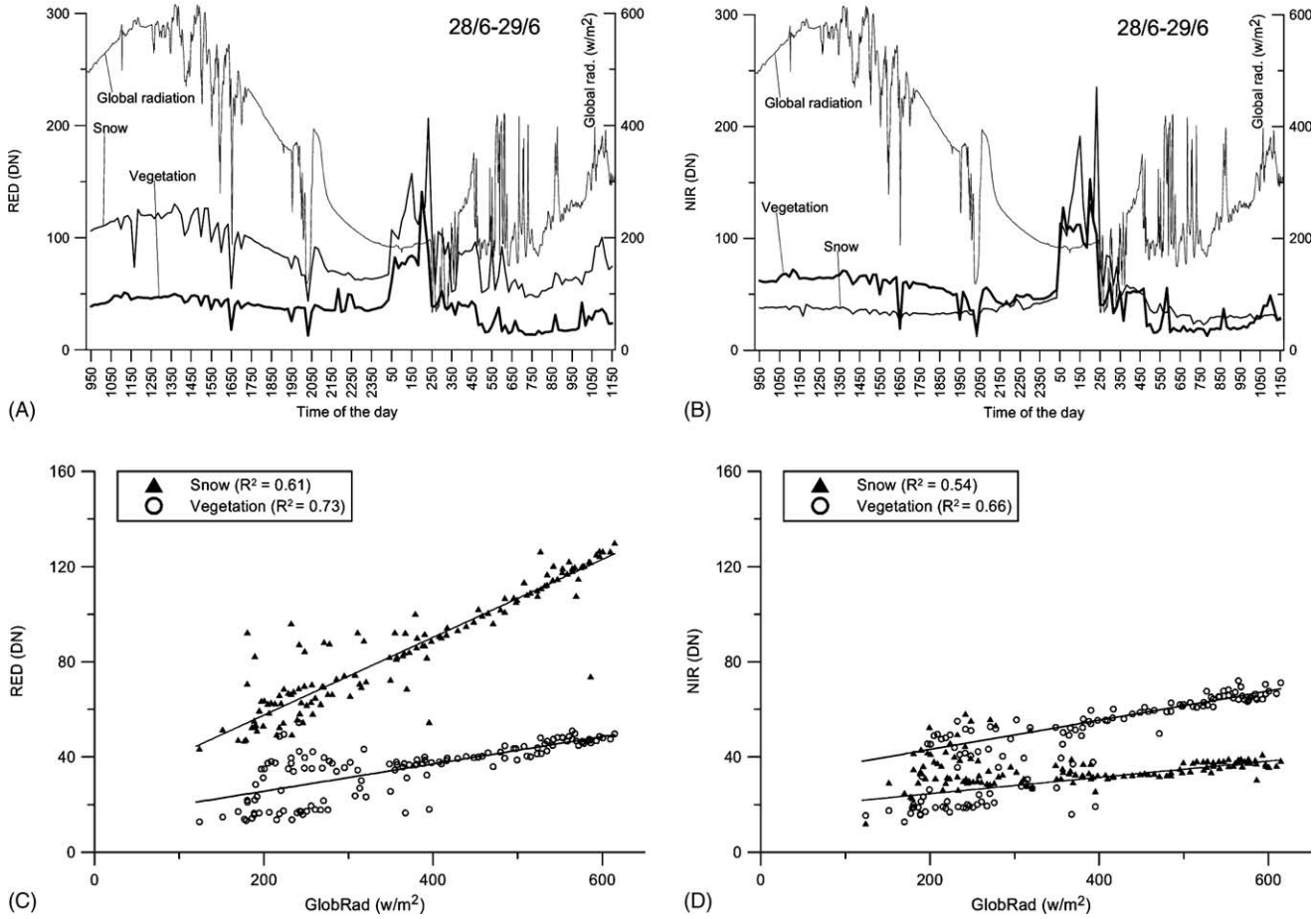

Fig. 3. Pixel values (snow and vegetation) from the diurnal (June 28–29) time series of multispectral camera images. (A, B) shows camera response (pixel values) in *R* and NIR and global radiation during the day. (C, D) shows *R* and NIR pixel values (period 21:00-04:00 excluded) plotted against global radiation.

meter covering the visible/near-infrared (VNIR) wavelength range from 350 to 1050 nm. The optical detector (which simply consists of the bare optical fibre with an adapter limiting the field of view to 18°) was fastened to a standard camera tripod to avoid movements during the less than one-second integration time of the measurement, and measurements were acquired 50 cm above the surface of interest. The spectral albedo was determined as the ratio of incident solar radiation reflected from the surface target and the incident radiation reflected from a calibrated white reference Spectralon plate (about 30 cm × 30 cm). Both the spectroradiometer and the reference Spectralon were calibrated at the optical calibration lab in Ny-Ålesund to "NIST traceable reference lamps and spectralons".

Measurements were done on representative snow and ice surfaces as well as typical vegetation, bare-soil/gravel, and particularly dark surfaces of former coal deposits (characteristics of spectral reflectance for different surface types are displayed in Fig. 2). Spectral reflectance measurements of the selected surfaces (snow, ice/water saturated snow, gravel, and vegetation) were performed at weekly intervals.

To be able to rectify image data orthographically, 16 ground control points (GCPs) were measured at visually significant spots in the Ny-Ålesund area (Fig. 4) using global positioning system (GPS).

4. Methods

4.1. Creating multispectral digital orthophotos

When the images are captured by the camera, they are created as a central projection of the object space (the real world) to the image plane (the CCD-chip in the camera). The central projection introduces displacements, which makes it impossible to measure the size of objects represented in the images. These displacements can be removed by performing a differential rectification of the images. The outcome of such a rectification is known as an orthophotograph or orthophoto. An orthophoto is basically an orthogonal projection of the objects in an image, and thus, all pixels in an orthophoto will all cover areas of equal size on the object plane. However, due to lens distortion, errors will arise in the

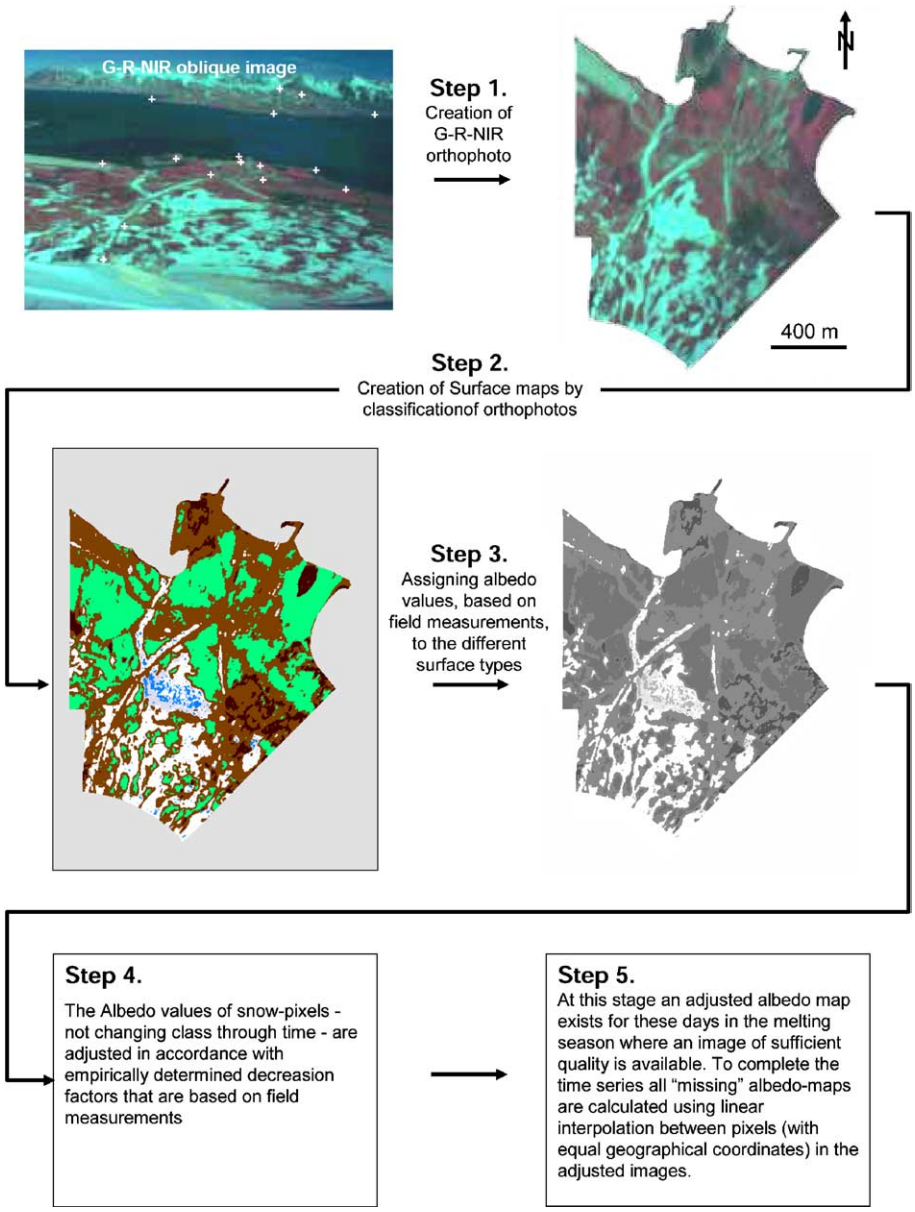

Fig. 4. Methodological sketch of the steps used in the procedure of transforming oblique image data into classified surface types and further into a full time series of albedo-maps. Ground control points (GCPs) used for geometric rectification are indicated with white crosses. On the classified map six surface types exist: snow (white), water saturated snow (blue), refrozen snow (light blue), vegetation (green), dark surfaces (dark brown), and gravel, etc. (brown).

orthophoto if distortion coefficients are not included in the rectification procedure. An exact camera calibration (Dueholm, 1989) therefore was performed in cooperation with the Technical University of Denmark (DTU).

To create the MDOs, the relation between the ground coordinate system and the image coordinate system must be known. When performing orthographic rectification using the software Ortho, this relation/transformation model is found using a digital elevation model (DEM) and a number of ground control points (GCPs). In this study orthographic rectification was based on the 16 GCPs collected during the field campaigns and a 20 m resolution DEM provided by the Norwegian Polar Institute (NPI). In order to improve the spatial resolution of the MDOs, the DEM was resampled to 4 m resolution. An example of an oblique multispectral digital image versus the corresponding MDO is illustrated in Fig. 4.

4.2. Classifying multispectral digital orthophotos into different surface types

The G, R, and NIR pixel values from the MDOs were used to classify the study area into maps representing six

different surface types: fresh snow, water saturated snow, metamorphosed/refrozen snow, vegetation, very dark surfaces e.g. former coal deposits, and gravel/intermediate reflective areas such as buildings, etc.

4.2.1. Classifying snow

As stated above, snow is divided into three distinct subclasses. However, in the first place all snow-pixels are selected using two empirically determined thresholds—both based on spectral reflective properties of gravel. In this study gravel is represented by the mean (raw pixel) value (in the image being processed) of the air strip situated in the upper left corner of the MDOs. The first step in the process of classifying snow involves two criteria:

$$\mathrm{NDSII} > 1.08 \cdot \mathrm{NDSII}_{\mathrm{Gravel}} \quad \text{and} \quad G > 0.8 \cdot G_{\mathrm{Gravel}}, \tag{2}$$

where G refers to raw green channel pixel values.

In order to divide snow into subclasses the following routine was introduced: The first step of the routine concerns the classification of water saturated snow. This class simply consists of pixels with an empirically determined NDSII threshold greater than 0.53. The classification of Metamorphosed/refrozen snow involves a throughput (in chronological order) of the whole time series of classified surface maps (at this stage including two snow-classes: fresh snow and water saturated snow). During the throughput it is checked whether pixels that are classified as fresh snow in the current surface map previously have been classified as water saturated snow. If this is the case, the given pixel will be assigned to the class of metamorphosed/refrozen snow.

4.2.2. Classifying vegetation, very dark surfaces, and gravel/intermediate reflective areas

Due to the strong reflectivity of green vegetation in NIR, a pixel simply can be classified as vegetation if its value in NIR is large relative to its value in VIS. For the Tetracam MDC it was empirically determined that pixels containing vegetation have a NIR to G (raw pixel values) ratio larger than 1.1.

Very dark surfaces are characterized by having a very low reflectance in all parts of the shortwave-spectrum. Thus, all pixels that are *not* vegetation (G significantly higher than NIR) and have an average GRNIR value $[(G+R+\mathrm{NIR})/3]$ significantly lower than gravel are assigned to this class. Thus, to classify this surface type the following two selection criteria were introduced:

$$G > 1.1 \cdot \mathrm{NIR} \quad \text{and}$$
$$[(G+R+\mathrm{NIR})/3] < 0.8 \cdot [(G+R+\mathrm{NIR})/3]_{\mathrm{Gravel}}, \tag{3}$$

where G, R, and NIR are raw pixel values in the red, green and near infrared channels, respectively.

Finally, if a pixel does not belong to any of the above mentioned classes, it is classified as gravel/intermediate reflective areas.

4.3. Deriving daily maps of broad band albedo

The total shortwave albedo has been measured routinely at the Norwegian Polar Institute research station in Ny-Ålesund since 1980 on the same tundra location (location 1 in Fig. 6). Eppley PSP Pyranometers and during the past 10 years Kipp and Zonen Pyranometers model CM11 have been used, annually calibrated on site with reference to the station Absolute Cavity Pyrheliometer. These measurements show that the albedo normally remains above 80% until late May. Thereafter, a rapid decrease in albedo occurs until albedo levels corresponding to snow-free tundra are reached (Winther et al., 1999). Basically, this decrease in albedo is related to two main factors—firstly, when the snow cover is thick enough not to be affected by the underlying ground, the decrease in albedo is due to snow melt and metamorphosis (increasing grain size), this albedo decrease occurs less rapidly than when the albedo is affected by the underlying ground. Secondly, at shallow snow depths (<10 cm), snow-albedo starts to get influenced by the ground, and at this stage the albedo decreases very rapidly, as the snow pack is thinning and is getting increasingly transparent. By combining this knowledge with the classified surface-maps and field measurements of surface reflectance, a method to calculate a time series of albedo-maps was developed. Using this method an albedo-map of the Ny-Ålesund area was derived for each day in the entire melting season.

Fig. 5 shows measured and calculated broad band albedo for a number of different surface types (snow, ice/water saturated snow, vegetation, and gravel). Furthermore two different albedo decrease coefficients ($0.804\%\,\mathrm{day}^{-1}$ and $0.567\%\,\mathrm{day}^{-1}$) are visualized in the figure. These coefficients are used to calculate albedo decrease for fresh and older/metamorphosed snow, respectively (when not affected by the underlying ground). All calculation routines included in the process of deriving albedo-maps, and all routines used for image classification during this study was programmed in chips scripting language (CSL), which is an integral part of the Copenhagen Image Processing System (CHIPS) developed at the Institute of Geography, University of Copenhagen (CDT, 2002). Below is given a systematic description of the derivation of the albedo-calculation routine: During the melting season, spectral surface reflectance was measured for the six surface classes. The spectral measurements were numerically integrated to broad band albedo. In the first place a time series consisting of 19 albedo-maps (derived from the classified MDOs) was created. During this process each surface type were assigned a particular albedo value based on

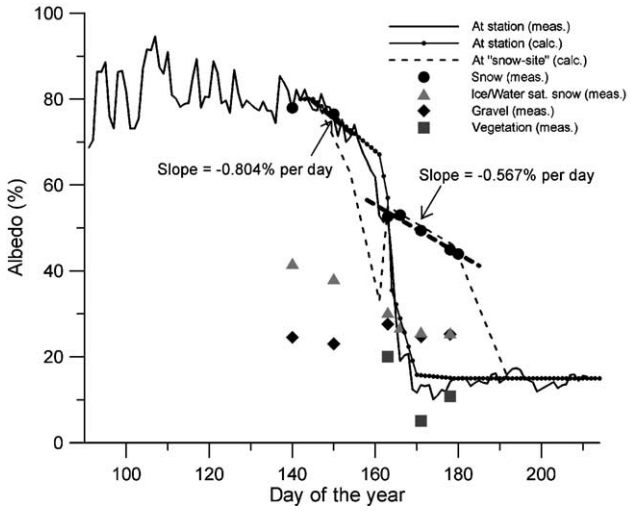

Fig. 5. Measured and modelled values of albedo at different dates. Measured data are from the NPIs research station and from spectral field measurements. Albedo decrease coefficients (fresh snow: $-0.804\%\,day^{-1}$ and metamorphosed snow: $-0.567\%\,day^{-1}$) are also indicated.

the numerically integrated values created from the field data: fresh snow: 80%, water saturated snow 33%, metamorphosed/refrozen snow: 55%, vegetation: 15%, very dark surfaces: 3%, and gravel/intermediate reflective areas: 23%. However, as discussed above; when the snow pack ages during the melting season, snow-albedo decreases with time; therefore snow-pixels in the 19 albedo-maps were recalculated using the above mentioned decrease factors for fresh and metamorphosed snow. The outcome of this procedure then is 19 new albedo-maps that are adjusted with respect to the age of the snow pack. The final step in calculating the time series was to fill the gaps of dates with missing albedo-maps. This was done using simple linear interpolation between pixels with equal geographical coordinates in the adjusted albedo-maps. The final output then come as a complete time series consisting of daily albedo-maps for the whole recording period/melting season (a sketch of the whole process from capturing the images to the production of daily albedo-maps is outlined in Fig. 4).

5. Results and analysis

In order to verify the accuracy of the derived albedo-maps, calculated and measured values of albedo were compared for the snow site where surface reflectance was measured regularly during/between the field campaigns; and for the permanent albedo monitoring station (Fig. 5). It can be observed that there is a good match between the calculated and the measured values. However, a high overall accuracy of the calculated results—spatially as well as temporally, requires, of course, that the classification of the MDOs is correct. Therefore, all classified surface-maps were checked by a careful visual inspection, and critical pixels (pixels that have been saturated one or more times during the recording period) were excluded from statistical calculations.

Fig. 6 presents a number of selected sites where data have been extracted from the calculated albedo-maps and Fig. 8 presents the change in albedo for these sites through time. These data, reflect that in the Ny-Ålesund area, the time it takes for the albedo to decrease from its maximum around 80% till it reaches bare ground levels varies a lot. It is also interesting to note that increases after a first decrease in albedo have occurred for a number of pixels corresponding to 14% of the areas with snow cover. At site 2 for example, surface runoff makes the snow pack water saturated (lowering the albedo) and dry out/refreezing processes makes the albedo increase afterwards. At site 7, the albedo decreases rapidly down to 30–40%, and thereafter it increases again until it reaches 50–60% before a new and last decrease. This phenomena is due to the presence of "naled ice" which is an ice body being formed by the refreezing of perennial ground water flow with snow accumulation on top of it (Lefauconnier, 2003, personal communication), the spring is located in an old mine named the Ester Mine and the main recharge of the sub-permafrost groundwater aquitar is the nearby Vestre Lovénbreen glacier (Haldorsen and Heim, 1999). When snowmelt is about to end (at this location by the beginning of July) the surface

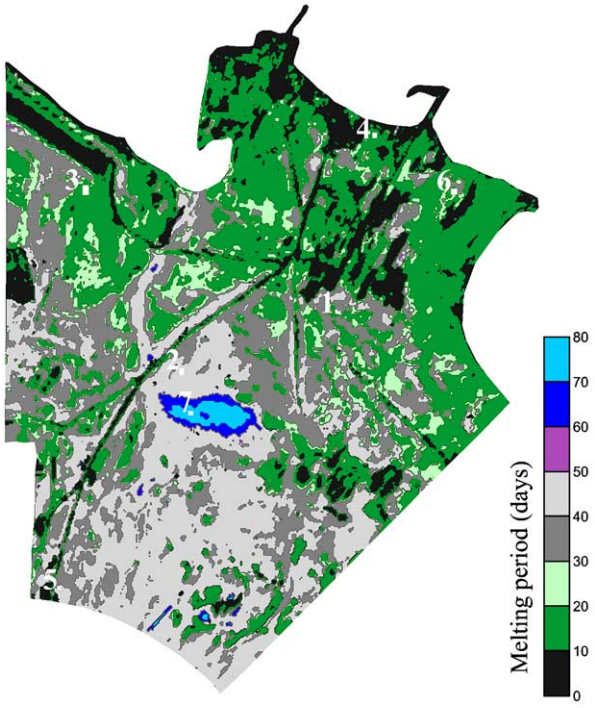

Fig. 6. Map displaying the spatial distribution of the duration of the snowmelt within the study area. Seven selected test sites are indicated on the map (corresponding curves of modelled albedo are shown in Fig. 8).

consists of ice made of a circular crystals overlapped by a layer of superimposed "dirty ice" and water saturated snow, making the albedo drop to around 35%. When the snow has disappeared, melting starts at the periphery of the crystals (especially with clear sky), and the drying of the surface and the increase of its roughness lead to an increase of the backscattering and of the albedo.

At the measurement site (close to the NPIs research station—location no. 1 in Fig. 6), the snowmelt season, defined as the period when albedo decreases from above 80% till it reaches bare ground level (<20%) has varied between 13 days in 1995 to 30 days in 1986, with an average of 23 days (Winther et al., 1999). Fig. 6 shows the spatial distribution of the length of snowmelt period in the Ny-Ålesund area (2002). The map was derived by running a throughput on the calculated albedo-maps, where the first day in the melting period is defined as the first day where the albedo gets below 80%, and the last day is defined as the day where it reaches its end value (vegetation, gravel, or dark "crust"). At the station, the derived snowmelt period lasts 23 days, indicating that with respect to the length of the snowmelt season, the year 2002 was very close to average. For the entire study area the average length of the 2002 melting season is 28.3 days with a standard deviation of 15.1 days (Fig. 7). However, from Fig. 6 it can also be observed that, spatially the length of the melting period varies a lot; from 0 days in areas where the snow is removed by human activity to between 70 and 80 days in areas with large accumulations of snow and ice. Further, it can be observed that the snow cover generally disappears most rapidly in areas close to the coast and nearby the Ny-Ålesund settlement.

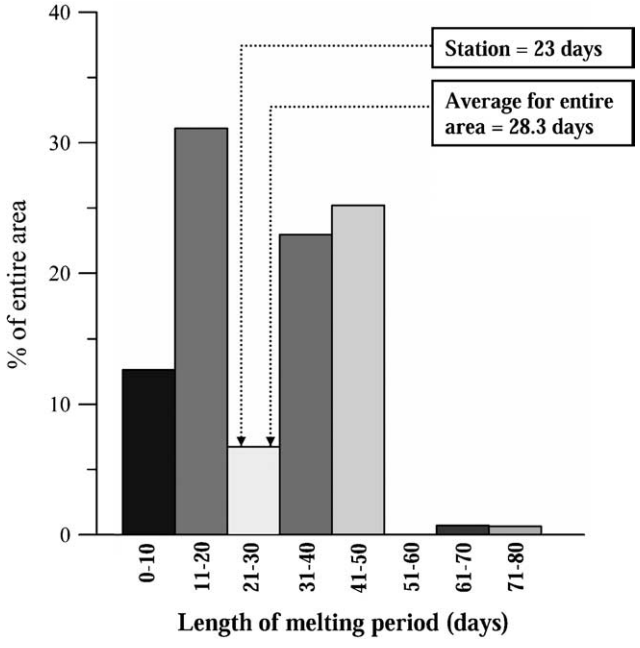

Fig. 7. The distribution of the duration of the melting period (eight temporal intervals) shown as percentages of the study area.

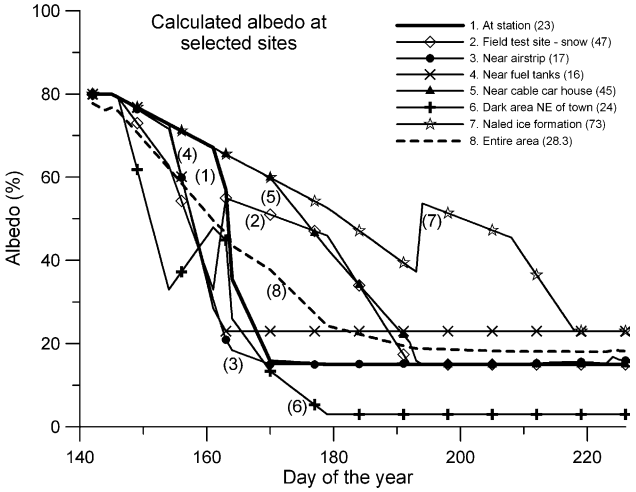

Fig. 8. Modelled surface albedo at selected test sites during the melting season. Numbers in parenthesises (in legend) indicate the modelled duration of snowmelt at the selected sites.

In Fig. 7 the distribution of the length of the melting season is given as percentage of the study area. The distribution was divided into 8 segments: 0–10 days (representing 12.6% of the area), 11–20 days (31.1%), 21–30 days (6.7%), 31–50 days (23.0%), 41–50 days (25.2%), 51–60 days (0.0%), 61–70 days (0.7%), and 70–80 days (0.6%). The figure describes a bimodal distribution indicating that during the melting season bare ground surfaces within the study area become free of snow in two main steps. The first step occurs early in the melting season before the 20th day and the second occurs in the last part of the season between the 30th and the 50th day. During the first step the majority of areas becoming snow-free are situated close to the coast/near the Ny-Ålesund settlement, indicating relatively shallow snow depths in these areas and possibly a higher concentration of impurities in the snow pack. Further, it is likely that areas located close to the coast are subjected to more drift and less accumulation. The second step primarily includes areas situated closer to the Zeppelin Mountain leading to the conclusion that a large amount of the snow-precipitation is drifting towards these areas forming a thicker snow pack. After around 50 days almost all of the snow/ice cover has disappeared except at one location situated in the central part of the study area, where a reservoir of snow/ice still is present after more than 60 days, and first after 80 days the area is 100% free of snow and ice. Finally, areas that are characterized by an intermediate melting period (20–30 days) only represent a relatively small fraction of the study area and though most of them are situated nearby the coast/Ny-Ålesund-settlement they generally seem to be almost stochastically distributed. This could indicate that they are small depressions with a slightly larger snow accumulation than the adjacent areas.

6. Conclusion and perspectives

During the snowmelt season the surface albedo in the Ny-Ålesund area decreases continuously (starting at 80%) until bare ground levels are reached when the tundra becomes free of snow. By utilizing knowledge of the spectral properties of different surface types and spectral ground measurements in combination with spectral image data; it was possible to develop a new method to give a detailed picture of this process. By using orthographic rectification on multispectral camera images, a set of geocoded image data with high spatial and temporal resolution was produced. The temporal resolution of these image data is significantly better than what can be obtained from high spatial resolution satellite remote sensing data. Due to varying weather conditions during the recording period the number of images suitable for surface classification was limited to 19 out of a total of 85. However this number of images is still high when compared to the fact that e.g. the Landsat TM/ETM (Thematic Mapper/Enhanced Thematic Mapper) satellite sensors overpasses the same area only a couple of times per month. The orthographically rectified multispectral images were transformed into maps representing different surface classes. These classified surface maps and the values of albedo measured in the field have made us able to create a methodology to produce a complete time series of daily albedo maps. The Time series covering the 2002 melting season reveals that duration of snow melt-off in the Ny-Ålesund area varies much in space and time. It seems that the tundra becomes free of snow in two main steps—one early in the season and one late in the season. Mostly, this can be explained by different snow accumulations (smallest near the coast and largest close to the mountainside). However, due to the presence of so called naled ice at one specific site, the duration of ice/snow coverage lasts significantly longer there than at all other sites. At some sites during melt-off, the surface albedo increases and is followed by an afterwards decrease. This phenomenon is due to the presence of the naled ice, surface runoff, and small accumulations of water, which lead to the formation of ice from refrozen water or water saturated snow packs with relatively low surface albedo. Dry-out and weathering of the ice crust lead to the afterwards increase in albedo.

This great variability, combined with the fact that Ny-Ålesund offers unique facilities for research/monitoring in the Arctic, favours the idea of future use of the technique discussed in this paper in long term environmental change monitoring programs in the area.

Furthermore, time series of daily albedo-maps could contribute to improve studies of surface energy balance modelling. In that context the Ny-Ålesund area could serve as representative for a typical coastal area in the region.

Finally, if modelled lengths of the melting period were combined with temperature data, the spatial distribution of snow cover thickness could be represented in form of degree days (transformed into snow water equivalents). These data then could be used in hydrological projects, e.g. estimation of the size water reservoirs represented by the snow cover.

Acknowledgements

This work was made possible under a grant from the European Commission IHP-programme (Ny-Ålesund Large Scale Facility, contract HPRI-CT-1999-00057). Further, the Norwegian Polar Institute is thanked for providing excellent facilities and data. Are Backlund, optical engineer at the Norwegian Polar Institutes research station (Sverdrup Station, Ny-Ålesund) is thanked for doing spectral measurements in between the field campaigns. Erik Poulsen and Ole Mærsk Møller, the Technical University of Denmark (DTU), Department of Informatics and Mathematical Modelling are thanked for doing the calibration of the camera-lens-distortion parameters. Finally, Kim Have former student at the DTU is thanked for developing the orthographical rectification software Ortho.

References

CDT (Chips Development Team), 2002. Online user's guide. Institute of Geography, University of Copenhagen. Available from <http://www.geogr.ku.dk/chips/index.htm>.

De Abreau, R., LeDrew, E., 1997. Monitoring Snow and Ice Conditions Using a Normalized Difference Index Based On AVHRR Channels 1 and 2. Available from <http://www.crysys.uwaterloo.ca/science/documents/ger97_deabreu2.pdf>.

Dozier, J., 1989. Spectral signature of Alpine snow cover from the Landsat Thematic Mapper. Remote Sensing of Environment 28, 9–22.

Dueholm, K.S., 1989. The generic bundle adjustment. US Geological Survey Open-File Report, pp. 89–185.

Haldorsen, S., Heim, M., 1999. An Arctic groundwater system and its dependence upon climatic change. An example from Svalbard. Permafrost and Periglacial Process 10, 137–149.

Hansen, B.U., 1991. Monitoring natural vegetation in southern Greenland using NOAA AVHRR and field measurements. Arctic 44 (1), 94–101.

Have, K., 1999. Photogrammetric image analysis for climate studies. Masters thesis, Department of Planning, The Technical University of Denmark, pp. 191, unpublished.

Hinkler, J., Pedersen, S.B., Rasch, M., Hansen, B.U., 2002. Automatic snow cover monitoring at high temporal and spatial resolution, using images taken by a standard digital camera. International Journal of Remote Sensing 23, 4669–4682.

Iqbal, M., 1983. An Introduction to Solar Radiation. Academic Press.

Jacobsen, A., Hansen, B.U., 1996. Estimation of the soil heat flux/net radiation ratio over high latitude natural vegetation using spectral vegetation indices. In: Proceedings of the Fourth Circumpolar Symposium on Remote Sensing of the Polar Environments, Lyngby 29 April–1 May 1996, pp. 33–38.

Jacobsen, A., Carstensen, A.R., Kamper, J., 1993. Mapping of satellite derived surface albedo on the Mitdluagkat Glacier, Eastern Greenland, using a digital elevation model and SPOT HRV data. Danish Journal of Geography 93, 6–18.

Lefauconnier, B., 2003. Personal communication.

Soegaard, H., Hasholt, B., Friborg, T., Nordstroem, C., 2001. Surface energy- and water balance in a high-arctic environment in NE Greenland. Theoretical and Applied Climatology 70, 35–51.

Tamstorf, M.P., 2000. Satellitbaseret vegetationskortlægning i Vestgrønland. Ph.D. thesis, pp. 177.

Warren, S.G., 1982. Optical properties of snow. Reviews of Geophysics and Space Physics 20, 67–89.

Winther, J.-G., Gerland, S., Ørbæk, J.B., Ivanov, B., Blanco, A., Boike, J., 1999. Spectral reflectance of melting snow in a high Arctic watershed on Svalbard: some implications for optical satellite remote sensing studies. Hydrological Processes 13, 2033–2049.

Wiscombe, W.J., Warren, S.G., 1980. A model for the spectral albedo of snow. I: Pure snow. Journal of the Atmospheric sciences 37, 2712–2733.